Understanding glycine conformation through molecular orbitals

Chantal T. Falzon and Feng Wang[a)]
Centre for Molecular Simulation, Swinburne University of Technology, P.O. Box 218, Hawthorn, Melbourne, Victoria 3122, Australia

(Received 21 September 2005; accepted 11 October 2005; published online 7 December 2005)

The four most stable C_s conformers of glycine have been investigated using a variety of quantum-mechanical methods based on Hartree-Fock theory, density-functional theory (B3LYP and statistical average of orbital potential), and electron propagation (OVGF) treatments. Information obtained from these models were analyzed in coordinate and momentum spaces using dual space analysis to provide insight based on orbitals into the bonding mechanisms of glycine conformers, which are generated by rotation of C–O(H) (II), C–C (III), and C–N (IV) bonds from the global minimum structure (I). Wave functions generated from the B3LYP/TZVP model revealed that each rotation produced a unique set of fingerprint orbitals that correspond to a specific group of outer valence orbitals, generally of a' symmetry. Orbitals $14a'$, $13a'$, $12a'$, and $11a'$ are identified as the fingerprint orbitals for the C–O(H) (II) rotation, whereas fingerprint orbitals for the C–C (III) bond rotation are located as $16a'$ [highest occupied molecular orbital (HOMO)], $15a'$ [next highest molecular occupied molecular orbital (NHOMO)], $14a'$, and $12a'$ orbitals. Fingerprint orbitals for IV generated by the combined rotations around the C–C, C–O(H), and C–N bonds are found as $16a'$, $15a'$, $14a'$, $13a'$, and $11a'$, as well as in orbitals $2a''$ and $1a''$. Orbital $14a'$ is identified as the fingerprint orbital for all three conformational processes, as it is the only orbital in the outer valence region which is significantly affected by the conformational processes regardless rotation of which bond. Binding energies, molecular geometries, and other molecular properties such as dipole moments calculated based on the specified treatments agree well with available experimental measurements and with previous theoretical calculation. © *2005 American Institute of Physics*.
[DOI: 10.1063/1.2133727]

I. INTRODUCTION

Gas-phase properties of molecules, such as amino acids, are fundamental to the understanding of complex structures, such as proteins and DNA, since many biological phenomena can be traced to fundamental properties of the molecular constituents. These properties are crucial for an understanding of intimate details surrounding the electronic charge redistributions in the outer valence orbitals during structural and conformational manipulations.

In addition to their biological significance as building blocks of peptides and proteins, amino acids are interesting species from a chemical point of view. For instance, the conformational flexibility associated with their backbone and side chains produces many local minimum structures on the torsional potential-energy surfaces of amino acids. As energy barriers associated with these conformational changes are typically large, these amino acids generally exist as single conformers. For other molecules, these energy barriers are quite small and isolation of a specific conformer is difficult. The conformational variety of amino acids is, however, imperative in determining the three-dimensional structure of proteins and thus controlling their dynamics.[1] Both laser spectroscopy and theoretical methods have made great contributions to elucidating the structures and dynamic of these biomolecules.[2]

Of the naturally occurring amino acids, glycine (NH_2CH_2COOH) is the simplest, but commonly serves as a model system for larger or more complex amino acids or proteins. It has been the subject of many studies, which include analysis of protein structure and folding and the role of interstellar amino acids in important prebiotic events.[3] The recent discovery of interstellar glycine, coupled with the ability to study the gas-phase properties of amino acids using electron momentum spectroscopy[4] (EMS) and resonant two-photon ionization (R2PI),[2] has been regarded as the first step in establishing the crucial link between amino acids in space and a pivotal role in the prebiotic chemistry of Earth.[5,6] Glycine is also a key participant in several reactions, including the biosynthesis of heme, an important constituent of hemoglobin and the biosyntheses of serine, purines (constituents of genetic materials), and glutathione (a coenzyme).[7]

The conformational behavior of glycine has brought many challenges to the experimental and theoretical investigations. The ability to generate flexible dihedral angles in protein structures has proven difficult for many methods.[4,8] Most theoretical work conducted on glycine has focused on the location of equilibrium geometries and determination of the relative energies of the glycine conformers. Theoretical studies have found as many as eight minimum-energy conformers present in the gas phase,[9] although a few of these conformers have been observed experimentally due to their thermal instability.[10] Predictions based on quantum-mechanical calculations are therefore essential in providing

[a)]Electronic mail: fwang@swin.edu.au

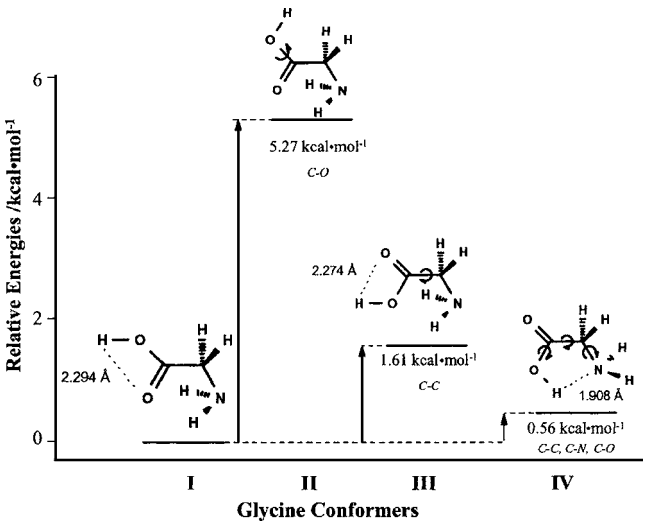

FIG. 1. Cross section of the torsional potential-energy surface for C_s glycine conformers calculated using the DFT-B3LYP/TZVP model.

details of individual conformers which experimental access is not yet achieved. Geometry and conformational characteristics of glycine were shown to be sensitive to the model used (the method and basis set).[4,8] Electron correlation effects play a significant role in the relative energies of the conformers,[11] where inclusion of polarization and diffuse functions in the basis sets were essential for geometry optimizations. This condition reflects in part the presence of several pairs of nonbonding electrons and intramolecular hydrogen bonding.[4] Sophisticated calculations using large basis sets and Møller-Plesset (MP) perturbation theory,[9] configuration-interaction (CI) methods,[12] or density-functional theory (DFT) methods including the Hartree-Fock (HF) exchange energy[3,8] yielded satisfactory agreement for not only geometries of conformers but also their relative energies. All calculations are consistent in the prediction that the C_s conformer (conformer I) depicted in Fig. 1 is the most populated and stable conformer of glycine.

The conformational processes of glycine in position space using both *ab initio* and DFT methods have been studied by Nguyen *et al.*[8] Subsequent work by Herrerd *et al.*[13] demonstrated that both B3LYP/6-311G** and MP2/6-311G** models were accurate descriptors of properties, such as geometrical parameters, conformational energies, and vertical ionization energies, in comparison with available experimental data, such as photoelectron spectroscopy (PES). Five of the lowest energy conformers of glycine, which are of C_s and C_1 symmetries all lie within 6 kcal mol^{-1} of the global minimum. Moreover, many conformationally induced shifts of the vertical ionization energies are described in terms of electrostatic and phase relationships in the associated Dyson orbitals,[13] but more quantitative information, for instance, from momentum space, on the Dyson orbitals of the conformers were not provided. Other experimental and computational works on glycine by Neville *et al.*[4] using EMS revealed that the inclusion of electron correlation was essential to describe long-range outer spatial regions of the electron density in the frontier orbitals of glycine. These workers focused on the synthesis of the observed orbital cross sections of glycine conformers in momentum space,[4] but provided no further structural information revealing the conformation processes and orbital fingerprints generated by rotations of the C–O(H), C–C, and C–N bonds of glycine.

With the presence of several stable conformers of glycine in the gas phase, a comprehensive understanding of the electron density distribution in the outer valence space of the conformers is therefore imperative. The objective of this investigation is to provide a unique orbital-based perspective of the electronic environment within those C_s conformers of glycine in both coordinate and momentum spaces. We concentrate on information that could differentiate each of the four conformers, such as equilibrium geometries and energies, vertical ionization energies (VIEs), molecular electrostatic potentials (MEPs), dipole moments, and orbital momentum distributions (MDs), using a technique known as dual space analysis (DSA).[14] This technique has been instrumental in the identification of orbital fingerprints for chemically interesting conformers, such as *n*-butane.[15,16] In particular, conformational variations in energies and orbitals are discussed in relation to rotations about the C–O(H), C–C, and C–N bond rotations of glycine, in order to provide a unique orbital-dependent representation of the bonding mechanisms within each conformer.

II. METHODS AND COMPUTATIONAL DETAILS

DFT with the hybrid B3LYP/TZVP model was employed to optimize the ground electronic states ($X\ ^1A'$) of the four C_s conformers of glycine presented in Fig. 1 (conformers I, II, III, and IV). The basis set used for conformation optimization is the triple zeta valence-polarized (TZVP) basis set of Godbout *et al.*[17] The B3LYP/TZVP model has been proven reliable for a number of molecular systems.[14–16,18–23] Based on the individual conformer geometries, three parallel calculations, namely, RHF/TZVP, OVGF/TZVP, and DFT-SAOP/ATZP were conducted for molecular properties, such as outer valence VIEs and dipole moments. Here the OVGF/TZVP model is the outer valence electron propagator (Green's function) model.[24,25] The DFT-SAOP/ATZP model is the orbital-dependent statistical average of orbital potential (SAOP) functional.[26–28] The ATZP basis set is a Slater-type basis set that has recently been tested.[29] All electronic structural calculations including the RHF/TZVP, OVGF/TZVP, and DFT-SAOP/ATZP models were based on the B3LYP/TZVP-optimized geometries using computational chemistry packages such as GAUSSIAN03,[30] GAMESS-US03,[31] and the Amsterdam density-functional (ADF) suite of programs.[32]

Next, the molecular wave functions obtained from single point calculations at the B3LYP/TZVP//B3LYP/TZVP level of theory were mapped directly into momentum space as orbital MDs, applying the plane-wave impulse approximation (PWIA),[33] the Born-Oppenheimer approximation, and independent particle approximation. The electron momentum spectroscopic orbital cross sections for randomly orientated molecules are given by[33,34]

TABLE I. Comparison of optimized geometrical parameters for the four C_s conformers of glycine using the B3LYP/TZVP method with experimental data and previous theoretical calculations.

		This work[b]				B3LYP/6-311G**[c]			
Parameter	Expt.[a]	I	II	III	IV	I	II	III	IV[d]
C–C/Å	1.526	1.524	1.534	1.527	1.535	1.525	1.539	1.533	1.533
C═O/Å	1.205	1.204	1.197	1.204	1.207	1.225	1.219	1.223	1.207
C–O/Å	1.355	1.354	1.360	1.356	1.343	1.382	1.386	1.389	1.340
C–N/Å	1.467	1.451	1.449	1.453	1.472	1.474	1.473	1.474	1.466
O–H/Å	0.966	0.969	0.965	0.969	0.987	0.971	0.967	0.971	0.981
C–H/Å	1.081	1.095	1.097	1.094	1.092	1.091	1.094	1.092	1.093
N–H/Å	1.001	1.015	1.016	1.015	1.012	1.013	1.014	1.011	1.012
O–C═O/°	···	123.1	120.6	122.7	123.6	123.4	120.6	122.9	···
O═C–/°	125.1	124.5	124.1	124.4	122.6	126.1	124.4	127.6	122.3
O–C–C/°	112.1	111.5	115.3	112.9	113.8	110.5	115.3	110.5	113.9
C–C–N/°	112.1	115.5	115.6	119.2	111.6	113.2	113.2	116.7	111.3
H–O–C/°	112.3	106.9	110.3	106.2	104.9	108.4	110.7	107.8	103.9
H–C–H/°	107.0	105.5	105.4	105.3	106.6	106.4	107.0	106.0	107.4
H–N–C/°	113.3	109.6	109.3	110.3	112.4	109.7	109.4	110.0	112.0
H–N–H/°	110.3	105.5	105.3	106.2	109.4	106.8	106.5	106.8	107.6
H–C–C═O/°	···	123.0	122.9	55.8	57.0	···	···	···	···
H–N–C–C/°	···	57.7	57.4	58.5	−110.9	···	···	···	−110.5

[a]Based on Structure I, Ref. 38.
[b]Present work using the B3LYP/TZVP model.
[c]The B3LYP/6-311G** calculation was not undertaken for conformer IV in Ref. 13.
[d]The MP(full)/6-311++G** model, Ref. 9.

$$\sigma \propto \int d\Omega |\psi_j(\mathbf{p})|^2,$$

where the Dyson spin orbitals are approximated by Kohn-Sham orbitals, $\psi_j(\mathbf{p})$. $\mathbf{p}$ is known as the momentum of the target electron at the instant of ionization, which is a function of the azimuthal angle ϕ measurable in the EMS experiment.[33] The method is implemented in the AMOLD codes of Weigold and McCarthy.[33] The PWIA is a good approximation for valence orbitals[35] as confirmed by the EMS measurement for N_{20} sufficiently high impact energies.[36]

III. RESULTS AND DISCUSSION

A. Geometric correlation of the glycine C_s conformers

Of the four conformers of glycine presented in Fig. 1, conformer I is the most abundant (52.6%).[4] The second most populated C_s conformer (29.3%) is conformer III, which is considered to result from rotation about the C–C bond (180°). The least populated C_s conformer (II) (0.3%) is obtained by 180° rotation of the C–O(H) bond in conformer I. Conformer IV involves three such rotations referred to conformer I: rotation of the C–C, C–O(H), and C–N bonds. Optimized geometric parameters for these four conformers, based on the B3LYP/TZVP model, are given in Table I.

The geometrical details predicted by the B3LYP/TZVP model for conformer I agree satisfactorily with both experimental results[37] and previous theoretical predictions.[4,8,9,13] Bond lengths and angles describing the geometry of the carboxylic acid and amine functional groups lie within 0.02 Å and 5°, respectively, of the experimental values. Relative to values based on the B3LYP/6-311G** model[13] (again for conformer I), the present B3LYP/TZVP model produced geometric parameters with an improved description of almost all bond lengths and bond angles (except for the ∠HOC angle) of conformer I. Further inspection of the geometrical results obtained using these two models reveals that the B3LYP/6-311G** model achieved a slightly superior agreement on nonoxygen related bond lengths and angles with the available experimental values.[37] This might indicate that the TZVP basis set is able to produce more accurate results to oxygen than the 6-311G** basis set. The hydrogen atom in the OH group may form an intramolecular H bond to the oxygen atom in the C═O group with a H···O distance of 2.294 Å according to the B3LYP/TZVP model.

Referring to conformer I, rotation of the C–O(H) bond (generating conformer II) produces only minor variations to bond lengths and angles connecting the C and O(H) atoms. This is highlighted by the underlined values in Table I. In a similar manner, negligible perturbations to the geometry occur as a result of rotation about the C–C bond (III). An exception is the ∠CCN angle, which undergoes a noticeable increase of 3.6° upon such a rotation (underlined in Table I). In contrast, generation of conformer IV, which requires a series of three rotations, forms a weak bond between the hydrogen atom of the OH group and the nitrogen atom of NH_2 (H···N distance is 1.908 Å), as indicated in Fig. 1. The C═O bond therefore becomes "isolated" and all related bonds and angles involving the C–C, C–N, C–O, and O–H bonds, are as a result, distorted to various degrees. An elongation (0.02 Å) of the O–H bond occurs, which can be considered as the result of inheritance from the C–C and C–O(H) rotations (III and II, respectively) plus the rotation of C–N; these changes have all been underlined in Table I.

TABLE II. Comparison of the molecular properties of the four C_s conformers of glycine using the B3LYP/TZVP model with other DFT and *ab initio* MP2 models.

Property	I[a]	II C–O	III C–C	IV C–O, C–C, C–N
ZPE/kcal mol^{-1}	49.83 (50.67)[b]	49.63 (50.40)[b]	49.88	50.06 (50.88)[b]
ΔE_{ZPE}/kcal mol^{-1}		5.27 (4.72)[c]	1.61 (1.59)[c]	0.56 (0.49)[d]
ΔE_{expt}/kcal mol^{-1}			0.9–1.5[e]	1.3–1.6[e] 1.4±0.4[f]
$\langle R^2 \rangle$/a.u.	425.5136	425.9568	421.0958	413.0627
Rotational constants				
A_e/MHz	10 300.5 (10 341.7)[g]	10 123.9 (10 136.1)[b]	9935.6 (9975.0)[b]	10 153.2 (10 175.1)[b]
B_e/MHz	3 837.2 (3 876.2)[g]	3 849.0 (3 885.0)[b]	3951.1 (3989.2)[b]	4 047.5 (4 076.3)[b]
C_e/MHz	2 886.9 (2 912.4)[g]	2 879.9 (2 901.4)[b]	2920.3 (2944.7)[b]	2 993.2 (3 010.9)[b]
Dipole moment				
μ_x/D	−0.8217	−2.7955	1.8089	−1.1399
μ_y/D	0.8727	−1.4046	−0.7267	−5.7457
μ/D	1.1987 (*1.2637*)[h] (1.1988)[i]	3.1285 (*3.3183*)	1.9494 (*1.9807*)[h]	5.8577 (*5.8769*)[h] (5.6892)[i]
Expt./D	1.0–1.4[j]			4.5–4.6[k]

[a]Total energy of conformer I is −284.534 123 6 E_h using the present B3LYP/TZVP model.
[b]MP2(full)/6-311++G**, Ref. 9.
[c]MP2/6-311G**, Ref. 13.
[d]MP2/6-311++G**, Ref. 4.
[e]Infrared spectroscopy of glycine (140–150 °C) isolated in an inert gas matrix, Ref. 43.
[f]Microwave spectroscopy (170–180 °C), Ref. 44.
[g]Electron diffraction, Ref. Note that theoretical rotational constants refer to equilibrium A_e, B_e, and C_e values, while experimental constants are A_0, B_0, and C_0, referring to zero vibrational energy level.
[h]SAOP/ATZP model used in present study.
[i]B3LYP/trun-pVTZ model, Ref. 4.
[j]Suenram and Lovas (Ref. 44) determined μ_a of conformer I to be 1.0±0.15 D and $\mu_b \neq 0$, $\mu_b > \mu_a$.
[k]Brown *et al.* (Ref. 45) found μ_a of conformer I to be 1.0±0.15 D and $\mu_b \neq 0$, $\mu_b > \mu_a$.

B. Stability of the conformers

Table II details the relative energies for each glycine conformers, generated using the B3LYP/TZVP method. This table also includes previous DFT (B3LYP/6-311G**) (Ref. 13) and *ab initio* calculations (MP2/6-311++G**) (Ref. 4) for comparison. It is observed that all the methods presented in Table II predict the four C_s conformers to lie within 6 kcal mol^{-1} of each other, with conformer I representing the global minimum. The relative energies (ΔE) obtained with the B3LYP/TZVP model, including zero-point energy (ZPE) correction (see Table II), agreed well with values given by the MP2/6-311G** model. The calculated relative energies including ZPEs between conformers I with II, III, and IV are predicted to be 5.27, 1.61, and 0.56 kcal mol^{-1}, respectively, which are in satisfactory agreement with values of 4.72 (II), 1.59 (III), and 0.49 kcal mol^{-1} (IV) predicted by the MP2/6-311G** method, and 5.72 and 1.59 kcal mol^{-1} for I–II and I–III, respectively, using the B3LYP/6-311G** model.[13] The relative energies of the glycine conformers are strongly influenced by the interplay of various intramolecular hydrogen bonding and *cis* or *trans* arrangement of the carboxylic acid (OH) within these conformers (refer to Fig. 1). The energy trend of I < IV < III < II remains consistent with previous theoretical calculations.[4,9,13]

The ΔE's, which were mapped into Fig. 1, highlight the energy positions on the cross sections of the torsional potential-energy surface of glycine. In this figure, conformer II possesses the highest-energy barrier as it barely forms any in-plane intramolecular H bonding. Though exhibiting the second lowest energy, conformer IV is only 0.56 kcal mol^{-1} greater than the global minimum I. The strong intramolecular interactions between H (in the OH group) and the lone pair of electrons on the nitrogen atom in the NH_2 group (with a separation of 1.908 Å) contribute to a decreased energy of this conformer (IV). The third most stable conformation in this study is conformer III (Fig. 1), which also possesses an in-plane intramolecular H bond. However, unlike the H···N bond in IV, the intramolecular H bond in conformer III is O–H···O=C. The H···O distance in III was predicted to be 2.279 Å, which is slightly shorter (0.015 Å) than the H···O distance predicted for I (2.294 Å), indicating a stronger H bond in conformer III. This stabilization is overshadowed by the C–C torsional strain present within III, thus serving to increase the overall conformational energy. In contrast, formation of conformer II breaks the in-plane H bond existing in conformer I, which produces isolation of the OH group. The lack of in-plane H bonding in this conformation may be the main reason why this conformer is located in a position with higher energy on torsional potential-energy surface (Fig. 1). The energetic nature and abundance of conformers

II and III are explicable via their orbital topologies, which are discussed in further detail later. The orbitals relating rotations of the C–O(H) (II) and C–C (III) bonds sit in two differing energy bands, with the former rotation located in the higher-energy band (13–18 eV). From an orbital perspective therefore, rotation of the C–C bond is energetically more achievable than rotation of the C–O(H) bond, thus formation of conformer III is energetically more favorable over II.

The natural abundances of these C_s conformers are in reverse of their predicted energy order. For example, the natural abundance of conformer III is predicted to be 29.3% compared to 9.0% for the lower-energy conformer IV. As seen in Fig. 1, this result is from the absence of a direct pathway on the torsional potential-energy surface for the global minimum structure I to enter the local minimum structure IV. Instead, to reach IV conformer I would almost certainly choose the lower-energy pathway of $I \rightarrow III \rightarrow IV$, rather than follow the higher-energy pathway of $I \rightarrow II \rightarrow IV$. Once conformer I has accumulated sufficient energy ($\Delta E = 1.61$ kcal mol^{-1}) to climb up to position III, it would drop into the local minimum well of III. Without sufficient energy, conformer III would not cross an energy barrier formed by the strain of rotating the C–O and C–N bonds to reach IV.

C. Conformational impact on molecular properties

Biomolecular conformers that differ by small energies can exhibit profound differences in their spatial and anisotropic properties, chemical bonding mechanism, and reactivity. Features such as electronic spatial extent $\langle R^2 \rangle$, rotational constants, and dipole moments are all important molecular properties for protein structure recognition and drug design. The molecular properties of the four C_s conformers of glycine are presented in Table II. Electronic spatial extent $\langle R^2 \rangle$ links with the size of conformers. The four conformers examined in this study have similar spatial extent, but conformers with in-plane H bonding (I, III, and IV) possess a size slightly smaller than species (II) without such bonding. The similarity in molecular volume yields flexibility of the glycine side chain in proteins. The rotational constants indicate that all conformers in the table are asymmetric rotors. This result agrees well with available experiments of I and IV. Theoretical rotational constants refer to equilibrium A_e, B_e, and C_e whereas experimental rotational constants are vibrationally averaged values of A_0, B_0, and C_0 (ν=0). Corrections used to obtain equilibrium rotational constants from the observed constants and correspond to the vibrational ground state are expected to be within several megahertz. However, the vibrational correction to the rotational constant of conformer I (Ref. 37) reduced the discrepancies between the theory and experiment.

In addition to size and three-dimensional similarities (important in protein docking), the accuracy of molecular wave functions is also ensured through consideration of various properties presented in different regions of space. These include energetic properties, such as the total energy (measurement in a small r region near the equilibrium), dipole moments (medium r region), and EMS orbital momentum distributions (large r region).[4] Dipole moments are the next key property in the study of these biomolecular structures, as it provides the degree and direction of electron charge distribution and polarizability within each conformation. The C_s glycine conformers given in Fig. 1 possess a planar symmetry (backbone atoms) there is no component of dipole moment along the z axis perpendicular to the plane. The substantial changes in dipole moment with respect to the single bond rotations are detailed in Table I. A large charge redistribution arises mainly when rotation occurs about the C–O(H) and C–N bonds. This is highlighted in conformers I, II, and IV, where dipole moments of 1.1987, 3.1285, and 5.8577 D, respectively, were predicted using the B3LYP/TZVP model. The dipole moments predicted in the present work agree well with 1.1987 (I), 3.3183 (II), 1.9807 (III), and 5.8769 D (IV) obtained when using the SAOP/ATZP model. Dipole moments of I and IV also agreed satisfactorily with 1.1988 and 5.6892 D calculated by Neville *et al.*[4] using the B3LYP/trun-pVTZ model. Among these conformers the dipole moment changes the least with respect to the rotation of C–C bond: 1.1987 D for conformer I compared to 1.9494 D for conformer III, but the vector components, μ_x and μ_y of III have altered considerably. For example, the μ_x of I is −0.8217 D and becomes 1.8089 D in III indicating significant charge redistribution to accommodate such a rotation. All rotations of the C–C, C–O(H), and C–N bonds consequently produce significant electron charge redistributions (sign and magnitude), as shown in Table II.

From further analysis of the impact of each conformational process, Fig. 2 provides information on the MEPs of the four conformations. The molecular plane of C_s conformers is defined as the backbone containing the C═O, C–O(H), C–C, and C–N bonds. The O–H bond of the carboxylic acid is also aligned within this plane, while the C–H and N–H bonds lie on both sides of the molecular plane, which serves as the reflection plane. The MEPs provided in Fig. 2 confirm significant electron charge redistribution in each conformer, as a consequence of the various conformational processes. In conformers I, II, and IV, the proton of the hydroxyl group (OH) deposits intensive positive charges (solid contours) at the interface where the oxygen and nitrogen atoms deposit intensive negative charges to form H bonds in I, III, and IV. This does not occur in II as the hydrogen atoms in the OH and CH groups are isolated from negative charges. The hydrogen atoms in the NH_2 group of conformer IV lie without the molecular plane; their impact on the molecular plane is minor.

D. Conformer-dependent ionization energy spectra

The ground electronic states ($X\,^1A'$) of the four C_s glycine conformers are all closed-shell states with 20 doubly occupied molecular orbitals; 15 are valence molecular orbitals, with 11 orbitals of a' symmetry and 4 orbitals of a''

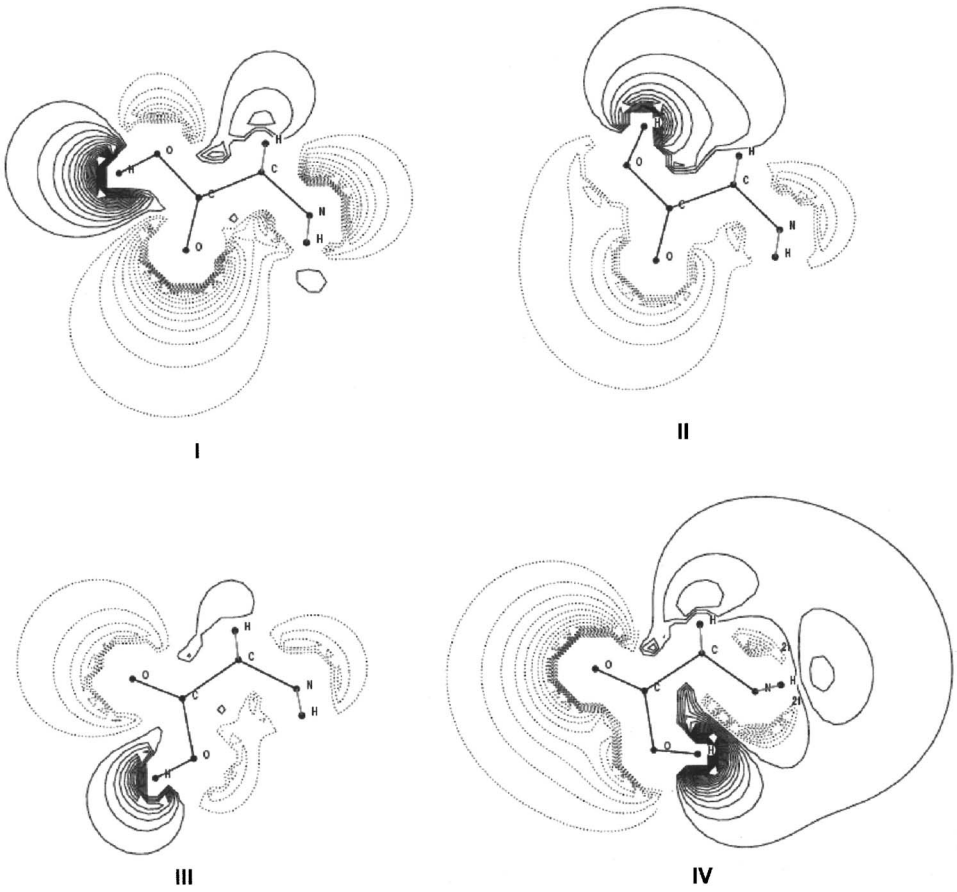

FIG. 2. Molecular electrostatic potentials (MEPs) of C_s conformers of glycine. The molecular plane is defined as the backbone connecting all the nonhydrogen atoms.

symmetry. The ten doubly occupied outer valence orbitals [plus the lowest unoccupied MO (LUMO)] of conformer I are given by both the B3LYP/TZVP//B3LYP/TZVP and the SAOP/ATZP//B3LYP/TZVP models as $(1a'')(11a')(12a')\times(2a'')(13a')(14a')(3a'')(4a'')(15a')(16a')(5a'')^0$. (Orbitals $1a''$ and $11a'$ in II are swapped, so are orbitals $3a''$ and $14a'$ in IV.)

Table III compares the vertical ionization energies of the outer valence orbitals in the region of 9–18 eV for the global minimum structure I, using the RHF/TZVP, OVGF/TZVP, and SAOP/ATZP models, with other theoretical results using the P3/6-311G** model[13] and available experimental data.[4,38–40] Ionization energies generated by the SAOP/ATZP and OVGF/TZVP models were generally found to agree well with the observed experimental spectra in almost the entire outer valence region. An exception is observed for the highest occupied molecular orbital (HOMO, $16a'$), where the SAOP method slightly overestimated the ionization energy by 0.4 eV, as seen in Table III. The semiempirical P3/6-311G** model[13] also agreed well with experiment but pro-

TABLE III. Outer valence ionization energies (eV) of glycine calculated using the RHF, DFT-SAOP, and OVGF models, together with available experimental results and a previous P3/6-311G** model for conformer I.

Orbital	SAOP/ATZP[a]	OVGF/TZVP (pole strength)	RHF/TZVP	P3/6-311G**[b]	Expt.[c]
$16a'$ (HOMO)	10.4 (10.5)	10.0 (0.93)	11.3	9.9	10(~10)[d]
$15a'$	11.4 (11.5)	11.4 (0.91)	12.8	11.0	11.1(~11.2)[d]
$4a''$	12.7 (12.7)	12.4 (0.91)	13.4	12.2	12.1(~12.2)[d]
$3a''$	13.5 (13.6)	13.6 (0.90)	14.6	13.5	13.6(~13.5)[d]
$14a'$	14.3 (14.4)	14.8 (0.92)	16.0	14.6	14.4(~14.2)[d]
$13a'$	15.0 (15.0)	15.1 (0.92)	16.5	14.8	15.0(~15.0)[d]
$2a''$	15.5 (15.5)	15.8 (0.91)	17.2	···	15.6
$12a'$	16.5 (16.5)	17.7 (0.91)	19.0	···	16.6
$11a'$	16.8 (16.8)	17.2 (0.90)	19.1	···	16.9
$1a''$	17.0 (17.1)	17.7 (0.91)	19.4	···	17.6

[a]Values based on the DFT-SAOP/TZ2P method are given in parentheses.
[b]P3/6-311G** model, Ref. 13.
[c]Photoelectron spectroscopy using He I (584 Å) and He II (304 Å) radiation lines, Ref. 38.
[d]He I Photoelectron spectroscopy, Ref. 39.

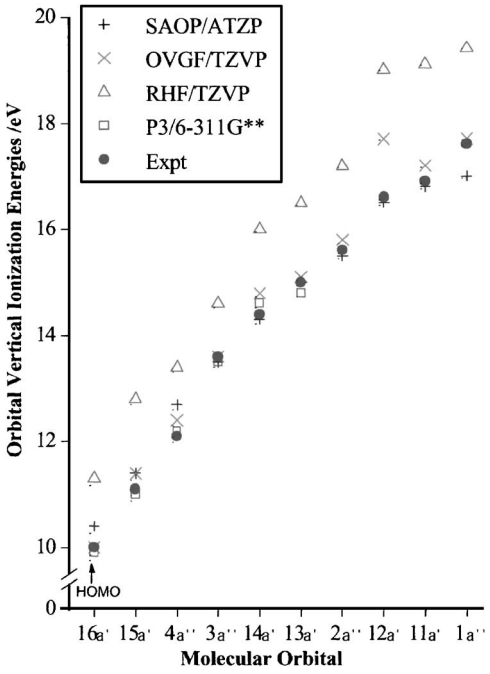

FIG. 3. A comparison of the binding energy spectrum of glycine (conformer I) with various models and the photoelectron spectroscopic experimental data.

duced energies of an incomplete set of outer valence orbitals. The discrepancies in the vertical ionization energy of HOMO are attributed to orbital relaxation and configuration effects, as indicated by the pole strengths (<1.0) determined in the OVGF calculations. The experimental binding (ionization) energies themselves are averaged values of all possible conformers existing under the experimental conditions, rather than a single conformer. Recent R2PI experiments[2] on *L*-phenylalanine have demonstrated that the conformer dependency on the binding energy of HOMO could range from 8.80 to 9.15 eV with a variation of approximately 0.35 eV. With this conformer dependence in the experimental binding energy spectra, the discrepancies between the present work and experimental work are therefore small. Furthermore, the present calculations have shown the domination of conformer I which "best" represents the experimental observations. The binding energies in the outer valence shell of I generated using various models and experiments are given in Fig. 3 as a benchmark of the calculations.

Deviations from experimentally measured VIEs indicate the presence of multiple low-lying energy conformations. Table IV lists the VIEs of the remaining three C_s conformers using these theoretical models. The SAOP model generates values for the orbital ionization energies consistent with values based on previous theoretical calculations. For conformers II and III, the ionization energies of the first three molecular orbitals predicted by the SAOP/ATZP model differed from those generated with the P3/6-311G** model[13] by 0.5 eV on average. This number decrease in the next three levels, where the discrepancy is less than 0.2 eV. No experimental binding energy spectrum is currently available for these conformers.

E. Outer valence orbital momentum distributions of the conformers

Properties obtained from coordinate space convey limited information about the variations of electronic structure associated with each conformational process.[13] Quantum mechanics is about energy and wave function.[14] Unlike the energetic properties, direct measurement of wave functions has been a challenge. The quality of wave functions has been indirectly assessed through molecular properties.[14] Until recently, EMS (Ref. 33) had been the most direct method to measure molecular wave functions (orbitals). The observation of the HOMO in the N_2 molecule using intense femtosecond laser pulsed on aligned molecules,[41] but luckily EMS will still dominate the measurement of wave functions until the new laser technique becomes applicable to larger and more complex systems such as amino acids and DNA bases.

In the present study, Dyson orbitals of each conformer have been calculated in coordinate space ($\boldsymbol{r}$ space) as orbital electron charge densities (CDs) and in momentum space (k space) as orbital MDs. Here we combine information obtained from both spaces (dual space analysis)[14] to provide insight into the electronic structure of each conformation as a result of the various conformational changes. Figure 4 reports the three outermost valence orbital MDs of glycine conformers with the experimental measurement.[4] Analogous to the coexistence of *trans*- and gauche-1,3-butadiene,[42] conformer signatures in the HOMO and NHOMO seen in Fig. 4 are likely those from other conformers in certain momentum regions. For example, appearance of conformer III in HOMO ($16a'$) is the region of $\phi<5°$. Furthermore, agreement of the simulated orbital MDs with the observed orbital MDs of orbital $4a''$ (Fig. 4) is better than those observed in the HOMO and NHOMO, if the experimental error bars are taken into account. This orbital is nearly invariant with respect to the rotations of the single bonds, which results in less scattered orbital MD measurements.

Figure 5 details all the symmetry-correlated (see Tables III and IV) outer valence orbital MDs for conformers I, II, III, and IV, with the orbital CDs of some representative orbitals of the conformer signature orbitals to be discussed in later sections. According to this figure all outer valence orbitals of these conformers experience, to some degree, distortion in their wave functions as a result of rotations. The exception is orbitals of a'' symmetry as they are related to the π bonding within each conformation. Any rotational process that occurs to the C_s conformation of glycine hence affects the in-plane s bonds rather than the out-of-plane p bonds. This phenomenon has been noted in the tautomerization process of the DNA base adenine.[23]

The orbitals $4a''$, $3a''$, $2a''$, and $1a''$, which are antisymmetric with respect to reflection in the molecular plane, are affected little by the conformational changes along the nodal plane. As a representative, the electron CDs of orbital $4a''$ of the conformers are provided in Fig. 5 ($4a''$). As highlighted in this figure, orbital $4a''$ is dominated by contributions from the C═O p bond formed by the $2p_z$ orbitals of oxygen and

TABLE IV. Outer valence ionization energies (eV) for conformers II, III, and IV calculated using the RHF, DFT-SAOP, and OVGF models.

Conformer	Orbital	SAOP/ATZP[a]	OVGF/TZVP (pole strength)	RHF/TZVP	P3/6-311G**[b]
II	16a'	10.5 (10.6)	10.0 (0.91)	11.4	10.0
	15a'	11.4 (11.5)	11.4 (0.91)	12.8	10.9
	4a''	12.6 (12.7)	12.3 (0.90)	13.3	12.0
	3a''	13.7 (13.8)	13.9 (0.92)	15.0	13.8
	14a'	14.4 (14.5)	14.7 (0.91)	16.1	14.7
	13a'	14.8 (14.9)	15.1 (0.90)	16.6	14.8
	2a''	15.5 (15.6)	15.8 (0.90)	17.2	···
	12a'	15.9 (16.0)	16.7 (0.91)	18.3	···
	1a''	17.2 (17.2)	17.9 (0.91)	19.2	···
	11a'	17.6 (17.6)	18.3 (0.90)	20.1	···
III	16a'	10.2 (10.3)	9.7 (0.91)	11.1	9.6
	15a'	11.8 (11.9)	12.3 (0.90)[c]	13.2	11.4
	4a''	12.5 (12.6)	11.9 (0.91)[c]	13.3	12.0
	3a''	13.6 (13.7)	13.7 (0.92)	14.9	13.6
	14a'	14.3 (14.3)	14.6 (0.92)	15.8	14.5
	13.a'	14.7 (14.8)	14.9 (0.92)	16.3	14.6
	2a''	15.5 (15.5)	15.8 (0.90)	17.2	···
	12a'	16.5 (16.5)	17.3 (0.90)	18.9	···
	11a'	16.6 (16.7)	17.8 (0.91)[c]	19.0	···
	1a''	17.0 (17.1)	17.6 (0.91)[c]	19.4	···
IV	16a'	10.6 (10.6)	10.0 (0.91)	11.4	···
	15a'	11.7 (11.8)	11.7 (0.90)[c]	12.6	···
	4a''	12.1 (12.2)	11.5 (0.91)[c]	12.9	···
	14a'	13.6 (13.6)	13.9 (0.92)[c]	15.2	···
	3a''	13.9 (14.0)	13.7 (0.91)[c]	15.3	···
	13a'	14.9 (15.0)	15.4 (0.91)	16.8	···
	2a''	15.5 (15.5)	15.8 (0.90)	17.1	···
	12a'	16.3 (16.3)	16.7 (0.91)	18.3	···
	1a''	17.3 (17.3)	18.0 (0.90)	19.9	···
	11a'	18.0 (18.0)	18.8 (0.91)	20.1	···

[a]Values based on the DFT-SAOP/TZ2P method are given in parentheses.
[b]P3/6-311G** model, Ref. 13.
[c]The marked pairs have energy flips as the orbital order is based upon the order of the DFT-SAOP/ATZP calculations.

carbon, as well as the $2p_z$ lone electron pair on the oxygen atom of the hydroxyl OH group. As both the C═O and C–O(H) bonds join at a common carbon, rotation by 180° about the C–O(H) single bond does not change the nature of this orbital. This orbital (4a'') in conformers I and II remains unchanged as indicated in their corresponding orbital MDs (solid line and dashed lines). In conformer III, some additional electron charge contribution is donated by the C–H pair from the CH_2 group. This can be considered as the small deviation in the orbital MD for III relative to the other conformers in the low-momentum region (the dotted line). The C–C bond orbital MD deviation in III has been compensated by the subsequent rotations of C–O(H) and C–N bonds in IV. Consequently, the corresponding orbital MDs of IV exhibit even smaller deviation in this region (the dash-dot line). In the same view, orbital 3a'' is a p-like bond formed by the lone pair of oxygen in C═O, CH_2, and NH_2. In this orbital the C–H pairs and N–H pairs serve as if each pair was a p orbital and the molecular plane is the nodal plane.

F. Orbital topology and chemical bonding of the C_s conformers

The low-resolution nature of EMS (1.5 eV) (Ref. 4) makes it difficult to fully resolve the entire spectrum of binding of glycine, because the splitting of ionization energies in outer valence shell is no more than 1.5 eV. High-resolution He II photoelectron spectroscopy (with resolution <0.3 eV) (Ref. 40) resolves this spectrum of glycine (see Table III for the energies). Only the outermost orbitals of 16a', 15a', and 4a'' in the region of 9–13 eV were fully resolved in the PES,[40] whereas the remaining seven outer valence orbitals in the region of 13–18 eV were partly resolved. In order to understand information pertinent to such a phenomenon, Fig. 6 provides the orbital topology of the four C_s conformers in the outer valence shell. In particular, the last band in the figure is a collection of all possible ionization energies of the C_s conformers deposited. An apparent energy gap (last column of Fig. 6) exists ($\sim$1.5 eV) between the third and fourth outermost orbitals (4a'' and 3a''), which, in turn, contributes to the separation of the 9–13 and 13–18 eV regions. In the

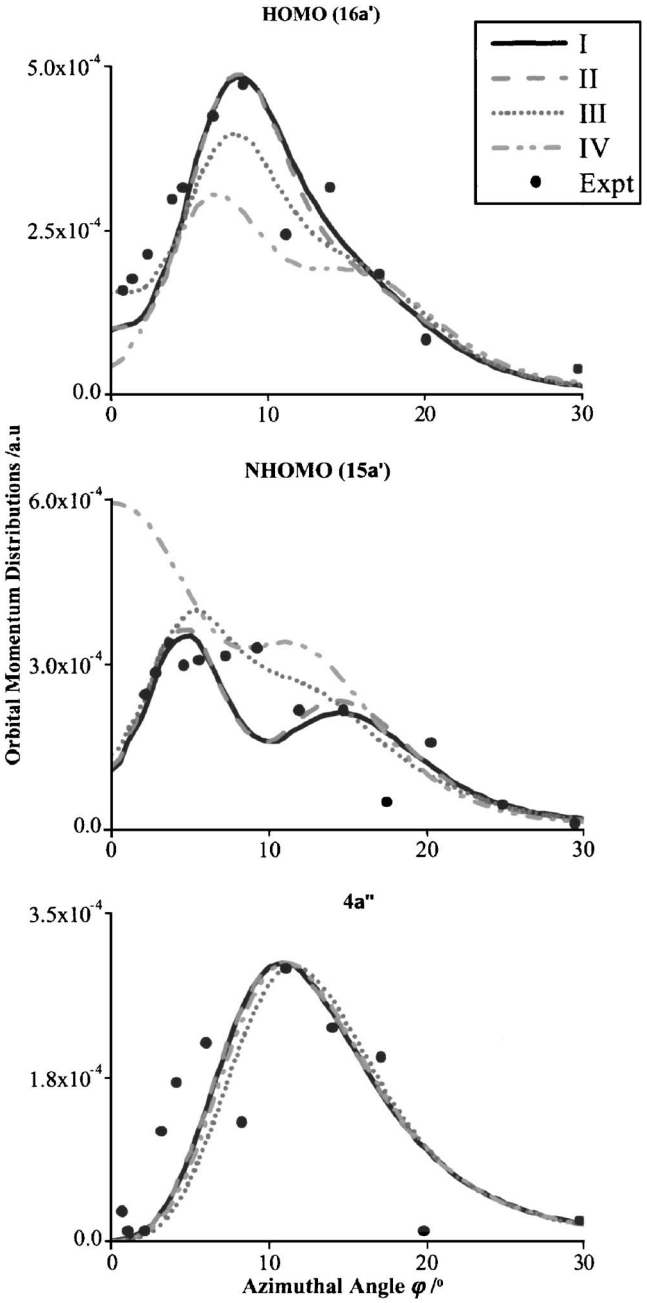

FIG. 4. A comparison of the experimental orbital momentum cross section (Ref. 4) with the synthetic orbital momentum distributions of the glycine conformers (I, II, III, and IV) for the fully resolved outermost orbitals of HOMO ($16a'$), NHOMO ($15a'$), and the third MO ($4a''$). The EMS experimental data were traced from Figs. 4, 6, and 7 of Ref. 4 as the original digital data are not accessible.

outermost region (9–13 eV), the orbital ionization energy splitting of orbitals $16a'$, $15a'$, and $4a''$ is sufficiently large enough to fit the resolution of PES, thus allowing for the detection of energies dominated by conformer I based on Boltzmann distribution. A consequence of the flexibility of the glycine backbone is the coexistence of other conformers with small energy splitting, in particular, conformers III and IV (and possibly other C_1 conformers). These conformers would populate and contribute to the binding energy spectrum of glycine under the experimental conditions. The last column of Fig. 6 provides the superposition energy spectrum of I+II+III+IV conformers. The energy levels in this region of 13–18 eV form an energy "band" and only very high-resolution spectrometers might resolve them. Conformer-dependent binding energy spectra of flexible amino acids have been reported experimentally using the R2PI technique.[2]

The orbital MDs presented in Fig. 5 indicate that in momentum space, it is possible to detect and differentiate molecular orbitals which are specific to individual conformational processes. As mentioned above the orbitals which show the most significant variation with conformation are dominated by a' orbitals; such orbitals are considered to be the fingerprints of rotation around a particular bond. The orbital fingerprints of a conformer (or rotation of a single bond with respect to conformer I) are identified when the individual orbital MDs are paired with the global minimum I, such that I+II, I+III, and I+IV. For example, rotation around the C–O(H) bond (II) causes significant changes to orbitals $14a'$, $13a'$, $12a'$, and $11a'$. These orbitals lie within the molecular plane and are dominated by σ bonds. In order to provide further insight into the orbital-based C–O(H) rotation, the orbital MDs and CDs of $14a'$ and $12a'$ for conformers I (solid curve) and II (dashed curve) are shown in the corresponding orbitals ($14a'$ and $12a'$) in Fig. 5. As seen in the figure, orbital $14a'$ of I exhibits a delocalized coverage on the H–O–C–C–N backbone with a strong $s^x p^y$ hybridization. Rotation of C–O(H) bond breaks this delocalized framework into isolated groups of O–C=O, C–C, and C–N. A significant reduction in the extent of p contribution to the $s^x p^y$ hybridization is thus observed in II, resulting in a more s dominant bond. In contrast, orbital $12a'$ is dominated by the lone pair of electrons on the oxygen atom of hydroxyl group, in addition to the significant contribution made from the density along the H–O–C=O bond in I. When rotation occurs, the strong s domination in I is diminished to an $s^x p^y$ hybridization in II, which, in turn, forms a more delocalized framework that is centered along the C–C bond and CH_2 group, as seen in the CDs of orbital $12a'$ in II.

Rotation of the C–C bond of I generates conformer III. In this case, significant orbital changes occur in the HOMO ($16a'$), NHOMO ($15a'$), $14a'$, and $12a'$ orbitals. The orbitals affected by this conformational process are all of a' symmetry. The orbital MDs and CDs of the HOMO ($16a'$) and orbital $12a'$ are given in the corresponding orbitals in Fig. 5 to illustrate the changes in the bonding nature between the two conformations. In both conformers, contribution in the HOMO is clearly made by the amine NH_2 group as well as $C-CH_2$. The C–N region does not have any noticeable density deposit and the charge deposited along the C–C bond is axial symmetric. Participation of the hydrogen atoms therefore contributes only to the s component of the $s^x p^y$ hybridization framework. Hence, the C–C rotation does not change the pattern of orbital MDs ($16a'$, dotted line) but rather reduces the contribution from the CH_2 group, as seen in the CDs of orbital $16a'$ of III. In comparison, orbital $12a'$ is dominated by contributions made in the region of H–O–C=O (I). Rotation of the C–C bond enhances electron concentration in this region and reduces the electron deposit in the C–C and $C-NH_2$ regions (orbital $12a'$, III).

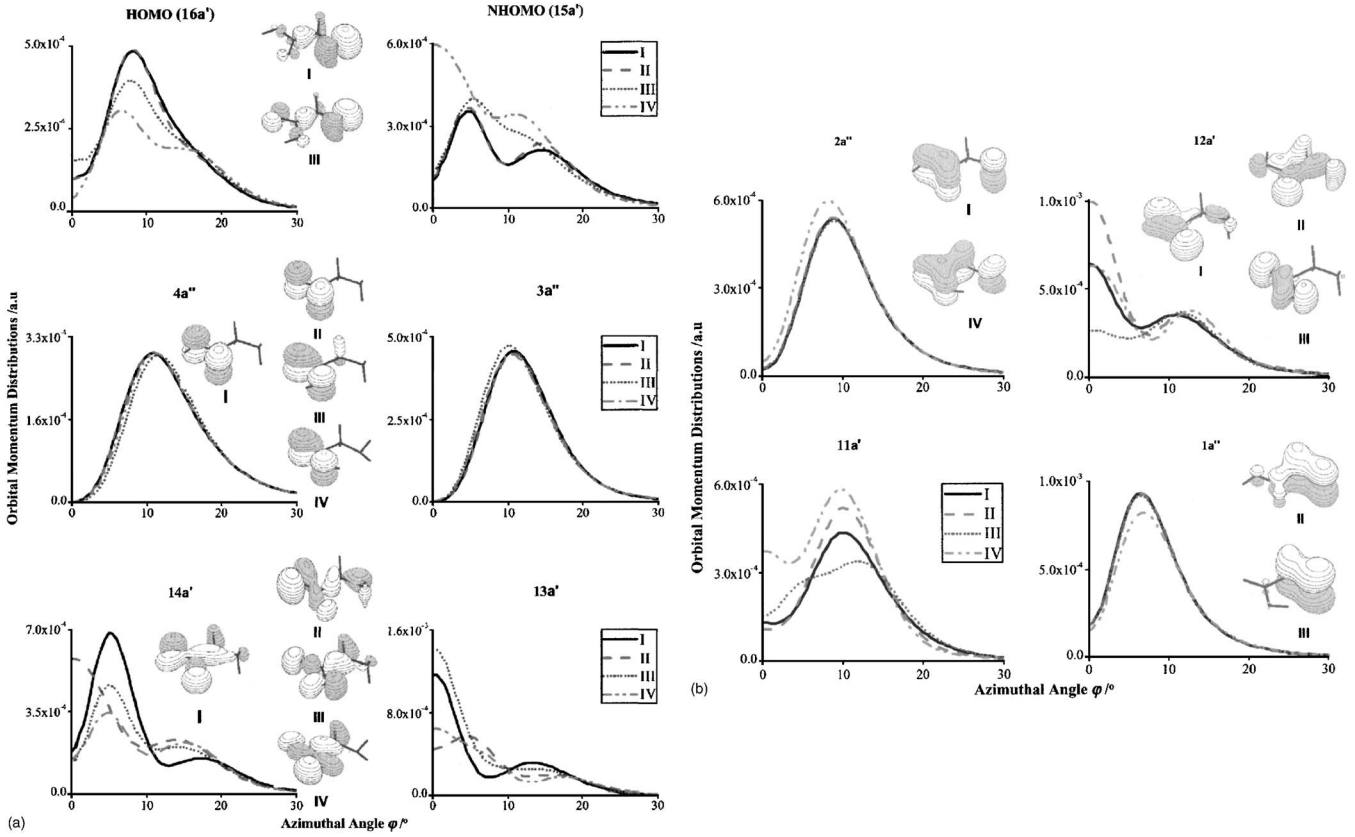

FIG. 5. [(a) and (b)] Simulated orbital MDs for all outer valence orbitals of glycine conformers I, II, III, and IV, together with the orbital electron charge densities (CDs) of representative orbitals of the conformers.

The strong *s* deduction (NH_2) resulted in the decrease of its orbital MD, as shown by dotted line in orbital $12a'$ of Fig. 5.

The combined rotations of the C–C, C–O(H), and C–N bonds within the C_s conformation of glycine (to generate IV) cause significant orbital variations in the HOMO ($16a'$), NHOMO ($15a'$), $14a'$, $13a'$, and $11a'$ orbitals, and in the $2a''$ and $1a''$ orbitals, while orbitals $4a''$, $3a''$, and $12a'$ are indistinguishable from those given for conformer I (see Fig. 5). The most pertinent observations within this conformation are that (1) orbital $14a'$ is the only orbital significantly affected by the conformational process, regardless of which bond was rotated, and (2) variations occur in the *p*-bonding orbitals $2a''$ and $1a''$. Orbital $14a'$ represents the culmination of rotations from conformers II [C–O(H)] and III (C–C). That is, this MO is affected by both the C–C and C–O(H) rotations. As mentioned above, the C–C rotation has its signature orbitals in the $16a'$, $15a'$ and $14a'$, $12a'$ orbitals (Fig. 5), while those affected by the C–O(H) bond rotation lie in orbitals $14a'$, $13a'$, $12a'$, and $11a'$. As MO $14a'$ changes with respect to *both* the C–C and C–O(H) rotations, this orbital is therefore considered as the orbital fingerprint for all nonhydrogen single bond rotations in glycine. The delocalized bond of orbital $14a'$ in conformer I is replaced by the more isolated antibonding nature in conformer II after the C–O(H) bond rotation. The orbital MDs of I and II are, as a result, very different. In the same manner, this orbital is different in conformer III as a result of the 180° rotation of the C–C bond in conformer I. Conformer IV can be considered as two rotations, i.e., C–O(H) and C–N from conformer III.

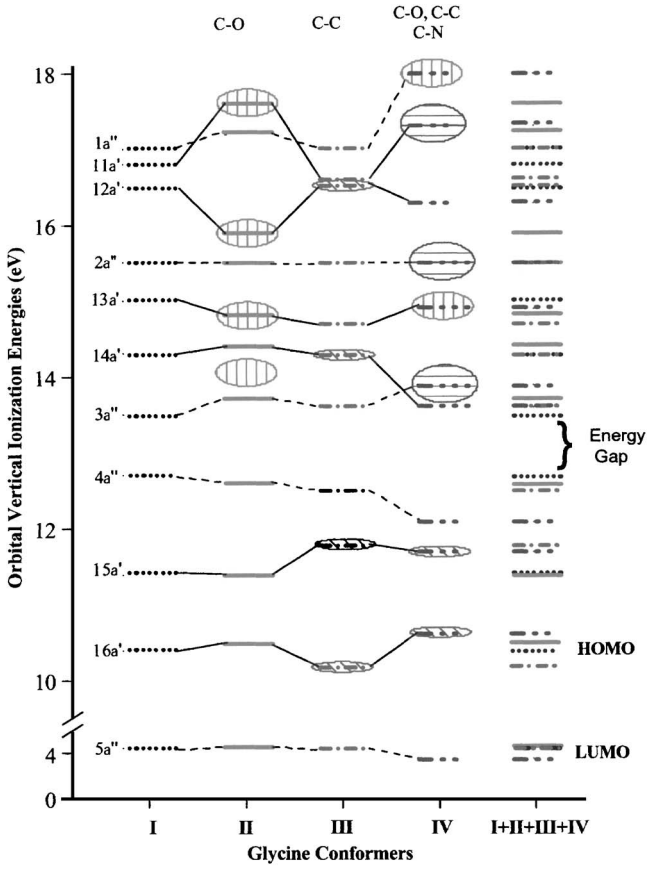

FIG. 6. Orbital topologies for the four C_s conformers of glycine in the outer valence region.

Rotation of the C–O(H) bond in III insignificantly alters the distributions of the orbital. In orbital $14a'$ the C–N bond is not populated. Therefore, rotation of this bond in conformer III causes no noticeable changes to the wave functions. The orbital charge densities of this orbital in conformers III and IV are therefore similar, which is reflected by their corresponding orbital MDs in Fig. 5.

Further observations of the orbital MDs for IV reveal that in orbital $12a'$ the consecutive rotations of C–C then C–O(H) (or vice versa) cause a cancelation of the effects on their related orbitals. The changes caused on rotating the C–O(H) (or C–C) bond are compensated by the rotation of the C–C [or C–O(H)] bond. As a consequence, orbital $12a'$ changed little, as indicated in Fig. 5 (solid line and dash-dot-dot line). Another unique characteristic to this conformer is that the *p*-bonding orbitals, $2a''$ and $1a''$, are the only orbitals of a'' symmetry that have responded to the single bond rotations. In conformer I orbital $2a''$ is delocalized, incorporating two isolated groups: (1) the amine-NH_2 group with the N–H bonds forming a *p*-like orbital and (2) from the $2p_z$ contributions of the atoms in the O═C−O moiety. The three consecutive single bond rotations to form IV (C–O, C–C, and C–N) do not affect the isolated nature of the NH_2 group but rather connects the C–C bond together with the CH_2 group, which is shown in Fig. 5 (orbital $2a''$ for I and IV). As a result, the $2a''$ orbital in IV is enhanced so that its MDs exhibit a larger spectroscopic pole strength (Fig. 5, orbital $2a''$, dash-dot-dot line). In contrast, orbital $1a''$ in I is a delocalized *p* bond that incorporates the H_2N-CH_2-C framework. When IV is generated this orbital becomes a more localized *p*-like bond which spans only over the H_2C-NH_2 bonding region (Fig. 5, orbital $1a''$ for IV), the spectroscopic pole strength of $1a''$ is therefore reduced, as indicated in Fig. 5 (MDs, orbital $1a''$).

IV. CONCLUSIONS

The four major C_s conformers of glycine have been studied with the Hartree-Fock theory (HF), density-functional theory with the hybrid B3LYP method, the SAOP models, and the Green's function theory. Information obtained from these models were combined with dual space analysis (DSA) to provide further insight into the bonding mechanisms of glycine on an orbital base, with respect to rotations of single bonds: C–O(H), C–C, and C–N bonds. Binding energies located using the SAOP and outer valence Green's function (GF) theory agree satisfactorily with available experimental measurements and previous calculations. The ionization energies calculated for the C_s conformers rationalize unresolved features, the photoelectron spectra, which are masked by superposition of the conformer-dependent ionization energies. Similarly, in momentum space, the momentum distributions of orbitals, such as $16a'$, $15a'$, and $14a'$ are likely to be conformer dependent.

Molecular geometries, energies, and dipole moments of each conformer obtained using the present models agree well with previous work and available experimental results. Such agreement indicates that the wave functions are sufficiently accurate in small *r* (total energies) and medium *r* (dipole moments) regions. Moreover, the extent of agreement with available experimental orbital cross sections (measured using EMS) indicates that the present wave functions are also accurate in larger *r* regions. The validated wave functions are therefore employed to investigate the conformations of glycine based on orbitals. The C_s conformational processes of glycine are produced on rotation of the C–C (II), C–O(H) (III), and C–C, C–O(H), and C–N (IV) single bonds from conformer I, with each rotation exhibiting fingerprints in a specific group of outer valence orbitals with a' symmetry. The antisymmetric *p* orbitals, i.e., $4a''$, $3a''$, $2a''$, and $1a''$ largely remained unchanged during these conformational variations.

Orbitals $14a'$, $13a'$, $12a'$, and $11a'$ were identified as the orbital fingerprints of C–O(H) (II) rotation, while the orbital fingerprints related to the C–C (III) rotation were found in the HOMO ($16a'$), NHOMO ($15a'$), $14a'$, and $12a'$ orbitals. The fingerprint orbitals, which result from the combination rotation of C–C, C–O(H), and C–N (IV), were to be found in orbitals $16a'$, $15a'$, $14a'$, $13a'$, and $11a'$ and in orbitals $2a''$ and $1a''$. Orbital $14a'$ in IV is considered to be the combination of corresponding orbitals from conformers II and III, whereas orbital $12a'$ corresponds to the "cancelation" of C–O(H) and C–C rotations. The most important orbital of the four conformers is orbital $14a'$, which represents a fingerprint orbital of all three rotations as it is the only orbital in the outer valence region to be significantly affected by all the conformational processes, regardless of which bond is rotated.

ACKNOWLEDGMENTS

The authors wish to acknowledge the Vice-Chancellor's Strategic Research Initiative Grant of Swinburne University of Technology and the Australian Partnership for Advanced Computing for using the National Supercomputing Facilities.

[1] J. M. Berg, J. L. Tymoczko, and L. Stryer, *Biochemistry*, 5th ed. (Freeman, New York, 2002).
[2] K. T. Lee, J. Sung, K. J. Lee, Y. D. Park, and S. K. Kim, Angew. Chem., Int. Ed. **41**, 4114 (2002).
[3] V. Barone, C. Adamo, and F. Lelj, J. Chem. Phys. **102**, 364 (1995).
[4] J. J. Neville, Y. Zheng, and C. E. Brion, J. Am. Chem. Soc. **118**, 10533 (1996).
[5] G. M. Muñoz Caro, U. J. Meierhenrich, W. A. Schutte, B. Barbier, A. Arcones Segovia, H. Rosenbauer, W. H.-P. Thiemann, A. Brack, and J. M. Greenberg, Nature (London) **416**, 403 (2002).
[6] Y. J. Kuan, S. B. Charnley, H. C. Huang, W. L. Tseng, and Z. Kisiel, Astrophys. J. **593**, 848 (2003).
[7] Glycine, (http://www.infoplease.com/ce6/sci/AO821060.html)
[8] D. T. Nguyen, A. C. Scheiner, J. W. Andzelm, S. Sirois, D. Salahub, and A. T. Hagler, J. Comput. Chem. **18**, 1609 (1997).
[9] A. G. Császár, J. Am. Chem. Soc. **114**, 9568 (1992).
[10] S. G. Stepanian, I. D. Reva, E. D. Radchenko, M. T. S. Rosado, M. L. T. S. Duarte, R. Fausto, and L. Adamowicz, J. Phys. Chem. A **102**, 1041 (1998).
[11] D. Yu, D. A. Armstrong, and A. Rauk, Can. J. Chem. **70**, 1762 (1992).
[12] C. H. Hu, M. Shen, and H. F. Schaefer III, J. Am. Chem. Soc. **115**, 2923 (1993).
[13] B. Hérrera, O. Dolgounitcheva, V. G. Zakrzewski, A. Toro-Labbé, and J. V. Ortiz, J. Phys. Chem. A **108**, 11703 (2004).
[14] F. Wang, J. Phys. Chem. A **107**, 10199 (2003).
[15] F. Wang and M. Downton, J. Phys. B **37**, 557 (2004).
[16] F. Wang and M. Downton, Chem. Phys. Lett. **384**, 144 (2004).
[17] N. Godbout, D. Salahub, J. Andzelm, and E. Wimmer, Can. J. Chem. **70**,

560 (1992).
[18] W. Adcock, M. J. Brunger, I. E. McCarthy, M. T. Michalewicz, W. von Niessen, F. Wang, E. Weigold, and D. A. Winkler, J. Am. Chem. Soc. **122**, 3892 (2002).
[19] F. Wang, H. Mackenzie-Ross, D. A. Winkler, I. E. McCarthy, L. Campbell, and M. J. Brunger, J. Comput. Chem. **22**, 1321 (2001).
[20] H. Mackenzie-Ross, M. J. Brunger, F. Wang *et al.*, J. Phys. Chem. A **106**, 9573 (2002).
[21] F. Wang, M. J. Brunger, I. E. McCarthy, and D. A. Winkler, Chem. Phys. Lett. **382**, 217 (2003).
[22] F. Wang, J. Mol. Struct.: THEOCHEM **728**, 31 (2005).
[23] F. Wang, M. Downton, and N. Kidwani, J. Theor. Comput. Chem. **4**, 247 (2005).
[24] L. S. Cederbaum and W. Domcke, Adv. Chem. Phys. **35**, 205 (1977).
[25] W. von Niessen, J. Schirmer, and L. S. Cederbaum, Comput. Phys. Rep. **1**, 57 (1984).
[26] O. V. Gritsenko, R. van Leeuwen, and E. J. Baerends, J. Chem. Phys. **101**, 8955 (1994).
[27] O. V. Gritsenko, R. van Leeuwan, and E. J. Baerends, Phys. Rev. A **52**, 1870 (1995).
[28] O. V. Gritsenko, P. R. T. Schipper, and E. J. Baerends, Chem. Phys. Lett. **302**, 199 (1995).
[29] C. T. Falzon, D. P. Chong, and F. Wang, J. Comput. Chem. (in press).
[30] M. J. Frisch, G. W. Trucks, H. B. Schlegel *et al.*, GAUSSIAN 03, Revision C.02, Gaussian Inc., Wallingford, CT, 2004.
[31] M. W. Schmidt, K. K. Baldridge, and J. A. Boatz, J. Comput. Chem. **14**, 1347 (1993).
[32] E. J. Baerends, J. Autschbach, A. Brces, C. Bo, P. M. Boerrigter, L. Cavallo, and D. P. Chong, ADF2004.01, Version 03, SCM, Vije Universiteit, Amsterdam, The Netherlands, 2003; http:www.scm.com..
[33] E. Weigold and I. E. McCarthy, Rep. Prog. Phys. **54**, 789 (1991).
[34] E. Weigold and I. E. McCarthy, *Electron Momentum Spectroscopy* (Kluwer-Academic, New York, 1999).
[35] S. A. C. Clark, T. J. Reddish, C. E. Brion, E. R. Davidson, and F. R. Frey, Chem. Phys. **143**, 1 (1990).
[36] Y. Khajuria, M. Takahashi, and Y. Udagawa, J. Electron Spectrosc. Relat. Phenom. **133**, 133 (2003).
[37] K. Iijima, K. Tanaka, and S. Onuma, J. Mol. Struct. **246**, 257 (1991).
[38] T. P. Debies and J. W. Rabalais, J. Electron Spectrosc. Relat. Phenom. **3**, 315 (1974).
[39] L. Klasinc, J. Electron Spectrosc. Relat. Phenom. **8**, 161 (1976).
[40] P. H. Cannington and N. S. Ham, J. Electron Spectrosc. Relat. Phenom. **32**, 139 (1983).
[41] J. Itatani, J. Levesque, D. Zeidler, H. Niikura, H. Pépin, J. C. Kieffer, P. Corkum, and D. M. Villeneuve, Nature (London) **432**, 867 (2004).
[42] S. Saha, F. Wang, C. T. Falzon, and M. J. Brunger, J. Chem. Phys. **123**, 124315 (2005).
[43] I. D. Reva, A. M. Plokhotnichenko, S. G. Stepanian, A. Ivanov, E. D. Radchenko, G. G. Sheina, and Y. P. Blagoi, Chem. Phys. Lett. **232**, 141 (1995).
[44] R. D. Suenram and F. J. Lovas, J. Am. Chem. Soc. **102**, 7180 (1980).
[45] R. D. Brown, P. D. Godfrey, J. W. V. Storey, and M.-P. Bassez, J. Chem. Soc., Chem. Commun. 547 (1978).